New Astronomy 16 (2011) 161–172

Contents lists available at ScienceDirect

New Astronomy

journal homepage: www.elsevier.com/locate/newast

First CCD *UBVI* photometric analysis of six open cluster candidates

A.E. Piatti [a,*], J.J. Clariá [b], A.V. Ahumada [b,c]

[a] Instituto de Astronomía y Física del Espacio, CC 67, Suc. 28, 1428 Ciudad de Buenos Aires, Argentina
[b] Observatorio Astronómico, Universidad Nacional de Córdoba, Laprida 854, 5000 Córdoba, Argentina
[c] European Southern Observatory, Alonso de Córdova 3107, Santiago, Chile

ARTICLE INFO

Article history:
Received 23 April 2010
Received in revised form 19 July 2010
Accepted 29 August 2010
Available online 6 September 2010
Communicated by J. Makino

Keywords:
Galaxy: open clusters and associations: general – open clusters and associations: individual: Haffner 3, Haffner 5, NGC 2368, Haffner 25, Hogg 3, Hogg 4
Galaxy: general – techniques: photometric

ABSTRACT

We have obtained CCD $UBVI_{KC}$ photometry down to V ∼ 22 for the open cluster candidates Haffner 3, Haffner 5, NGC 2368, Haffner 25, Hogg 3 and Hogg 4 and their surrounding fields. None of these objects have been photometrically studied so far. Our analysis shows that these stellar groups are not genuine open clusters since no clear main sequences or other meaningful features can be seen in their colour–magnitude and colour–colour diagrams. We checked for possible differential reddening across the studied fields that could be hiding the characteristics of real open clusters. However, the dust in the directions to these objects appears to be uniformly distributed. Moreover, star counts carried out within and outside the open cluster candidate fields do not support the hypothesis that these objects are real open clusters or even open cluster remnants.

1. Introduction

Among the 1787 currently catalogued open clusters[1] (OCs), more than half of them have been poorly studied or even unstudied up to this moment. Therefore, the mere confirmation of the physical reality of an OC candidate means significant contribution to get to know the Galactic OC system better. The current paper is thus part of a larger systematic survey whose goal is to obtain good-quality photometric data not only to enlarge the sample of studied OCs but also to estimate their fundamental parameters more accurately. This study represents a further step in a long-term project aimed at confirming the physical reality of catalogued OCs, to obtain the fundamental parameters of some unstudied OCs or to improve the quality of observationally determined properties for some poorly studied ones.

As it is commonly accepted, an apparent concentration of stars in the sky does not necessarily lead to the conclusion that such concentration constitutes a real physical cluster. The presence of such star concentration implies that we are dealing with a real physical system only in the case of globular clusters or very concentrated OCs. For most of the apparent star concentrations in the sky, however, it is necessary to have Supplementary information available about proper motions, radial velocities, spectral types and photometry to confirm their physical reality. The photometric data are often the only information at our disposal from which the existence of an OC may be inferred.

Any of the following factors, or a combination of them, could account for the presence of an apparent concentration of stars in a certain region of the sky: (i) the presence of a genuine OC, (ii) a chance grouping of stars along the line of sight or (iii) a non uniform distribution of interstellar material in that region of the sky. In the last few years, several CCD photometric studies of OC candidates included in Lyngå (1987) catalogue have been carried out with the main purpose of examining their nature to confirm whether or not they are genuine physical systems (see, e.g.,Piatti et al., 2000, and references therein). Even though in some cases the studied objects have been confirmed as real OCs (e.g., Piatti et al., 1998; Piatti et al., 2000), in some other cases, evidence was found supporting the fact that some objects catalogued as OCs are not real clusters but rather random fluctuations of the stellar density in a given region (see, e.g., Carraro and Patat, 1995; Piatti and Clariá, 2001a). The physical nature of some OC candidates is still arguable. A typical case is NGC 6994 that Bassino et al. (2000) considered a 2–3 Gyr OC. Carraro (2000), however, believed it to be simply a random enhancement of four bright stars above the background level. As star clusters are known to evolve dynamically and stellar depletion effects eventually lead to cluster disruption, some unconfirmed clusters are likely to be cluster remnants or fossil remains (de la Fuente Marcos, 1998; Bica et al., 2001).

In the present work, we try to clarify the nature of six catalogued OC candidates by using high-quality CCD $UBVI_{KC}$ photometry down

* Corresponding author.
E-mail addresses: andres@iafe.uba.ar (A.E. Piatti), claria@oac.uncor.edu (J.J. Clariá), aahumada@eso.org (A.V. Ahumada).

[1] http://www.astro.iag.usp.br/∼wilton

1384-1076/$ - see front matter © 2010 Elsevier B.V. All rights reserved.
doi:10.1016/j.newast.2010.08.009

Table 1
Parameters taken from the literature of the six catalogued open cluster candidates.

Cluster	α_{2000} (h m s)	δ_{2000} (° ′ ″)	l (°)	b (°)	Trumpler class[a]	Angular diameter (′)
Haffner 3	07 04 00	−06 08 00	219.8198	−00.0136	III2p	5.0
Haffner 5	07 18 02	−22 40 00	236.0715	−04.6249	II2m	7.0
NGC 2368	07 21 06	−10 22 18	225.5365	+01.7707	IV3p	3.0
Haffner 25	07 48 40	−25 57 00	242.3231	−00.1015	III1p	2.0
Hogg 3	09 57 39	−54 41 00	279.5071	+00.0838	IV2p	2.0
Hogg 4	09 57 45	−54 36 00	279.4675	+00.1586	–	4.0

[a] Taken from Archinal and Hynes (2003).

to $V \approx 22$ in the cluster fields. The selected OC candidates are Haffner 3 (OCl-556), Haffner 5 (OCl-624), NGC 2368 (OCl-571, Cr 138), Haffner 25 (OCl-656), Hogg 3 (OCl-794, ESO 167-12) and Hogg 4 (OCl-793). Additional designations above have been taken from Alter et al. (1970), Collinder (1931) and Lauberts (1982). Their corresponding equatorial and Galactic coordinates are given in Table 1, together with the Trumpler (1930) class according to Archinal and Hynes (2003) and the angular diameters taken from Lyngå (1987). Hogg 3 and Hogg 4 are located in Vela, Haffner 3 and NGC 2368 in Monoceros, Haffner 5 in Canis Major and Haffner 25 in Puppis. As far as we are aware, none of these OC candidates has ever been photometrically studied before.

The layout of this paper is as follows: Section 2 presents the observational material and the data reduction. In Section 3.1, we describe a method to filter the photometry from uniform patterns in terms of spatial density, magnitude and colour distributions and we apply photometric membership criteria to distinguish cluster members from field stars. In Section 3.2, we carry out star counts in the studied fields and clean the various extracted photometric diagrams of the cluster candidates from field star contamination. We also perform a statistical test that reflects the distribution of field fluctuations and stellar density contrast in the colour–magnitude diagrams between those in the clusters and those in the star fields. Section 3.3 deals with a few previous results on some of these objects. Finally, Section 4 summarizes our findings and conclusions.

2. Data collection and reduction

We obtained images of the suspected OCs during the nights of December 25, 27 and 29, 2000, with the $UBVI_{KC}$ filters and a 2048×2048 pixel Tektronix CCD attached to the 0.9 m telescope – scale of 0.4 arcsec pixel^{-1} – at Cerro Tololo Inter-American Observatory (CTIO, Chile). In order to standardize our photometry, we observed standard stars of the Selected Areas PG0231+051, 92 and 98 of Landolt (1992). By the end of each night, we had collected an average of 45 different measures of magnitude per filter for the selected standard star sample.

Table 2 shows the logbook of the observations with filters, exposure times, airmasses and seeing estimates. Observational setups, data reduction procedures, stellar point spread function photometry and the transformation to the standard system follow the same prescriptions described in detail in Piatti et al. (2009). The standard star photometry shows the root-mean-square deviation of the observations from the fits to be less than 0.015 mag, indicating that the nights were photometric. Once the standard magnitudes and colours were obtained, we built a master table containing the average of V, $U-B$, $B-V$, and $V-I$, their errors $\sigma(V)$, $\sigma(U-B)$, $\sigma(B-V)$ and $\sigma(V-I)$ and the number of observations for each star, respectively. Tables 3–7 present this information for Haffner 3, Haffner 5, NGC 2368, Haffner 25, Hogg 3 and Hogg 4, respectively. Only a portion of these tables is shown here for guidance as their form and content. Tables 3–7 are available in their entirety in the online version of the journal. The deepest CCD images obtained for the object sample are shown in Fig. 1.

Table 2
Observation log of selected clusters.

Cluster	Date	Filter	Exposure (s)	Airmass	Seeing (″)
Haffner 3	December 27, 2000	*B*	20	1.19	1.8
		B	60	1.19	2.1
		B	360	1.18	2.2
		V	20	1.17	1.7
		V	60	1.16	1.6
		V	200	1.16	1.7
		I	10	1.15	1.7
		I	10	1.15	1.3
		I	90	1.14	1.4
		U	60	1.14	1.8
		U	540	1.13	1.6
Haffner 5	December 27, 2000	*I*	10	1.01	1.1
		I	90	1.01	1.3
		B	20	1.01	1.4
		B	60	1.01	1.4
		B	360	1.01	1.5
		V	20	1.01	1.1
		V	60	1.01	1.3
		V	200	1.01	1.3
		U	60	1.01	1.6
		U	540	1.01	1.7
NGC 2368	December 25, 2000	*V*	20	1.07	1.7
		V	60	1.07	1.7
		V	200	1.07	1.6
		B	360	1.07	1.8
		B	60	1.06	2.0
		B	20	1.06	1.7
		I	10	1.06	2.0
		I	90	1.06	1.6
		U	60	1.06	2.2
		U	540	1.06	1.8
Haffner 25	December 29, 2000	*V*	20	1.00	1.2
		V	60	1.00	1.3
		V	200	1.00	1.4
		B	20	1.00	1.5
		B	60	1.00	1.4
		B	360	1.00	1.8
Hogg 3 and 4	December 25, 2000	*U*	60	1.10	2.4
		U	540	1.10	2.2
		B	20	1.10	2.5
		B	60	1.10	2.0
		B	360	1.10	2.0
		V	200	1.10	1.9
		V	60	1.10	2.2
		V	20	1.10	2.4
		I	10	1.10	1.7
		I	90	1.11	2.3
	December 29, 2000	*V*	20	1.11	1.3
		V	60	1.11	1.2
		V	200	1.11	1.3
		B	20	1.10	1.3
		B	60	1.10	1.5
		B	360	1.10	1.6
		I	10	1.10	1.2
		I	90	1.10	1.3
		U	60	1.10	1.4
		U	540	1.10	1.5

Tables 3–7 reveal that stars with three measures of $U-B$, $B-V$ and $V-I$ colours extend from the brightest limit down to

Table 3
CCD *UBVI* data of stars in the field of Haffner 3.

ID	x (pix)	y (pix)	V (mag)	$\sigma(V)$ (mag)	n_V	$U-B$ (mag)	$\sigma(U-B)$ (mag)	n_{UB}	$B-V$ (mag)	$\sigma(B-V)$ (mag)	n_{BV}	$V-I$ (mag)	$\sigma(V-I)$ (mag)	n_{VI}
	–	–	–	–	–	–	–	–	–	–	–	–	–	–
29	562.690	1091.613	12.031	0.004	3	2.009	0.002	2	1.575	0.003	2	1.585	0.048	3
30	1798.515	736.634	12.640	0.005	3	0.370	0.002	2	0.757	0.007	2	0.777	0.005	3
31	440.379	2038.542	12.836	0.039	3	0.530	0.000	1	0.907	0.013	2	0.889	0.012	3
	–	–	–	–	–	–	–	–	–	–	–	–	–	–

NOTE: (x,y) coordinates correspond to the reference system of Fig. 1. Magnitude and colour errors are the standard deviations of the mean or the observed photometric errors for stars with only one measurement.

Table 4
CCD *UBVI* data of stars in the field of Haffner 5.

ID	x (pix)	y (pix)	V (mag)	$\sigma(V)$ (mag)	n_V	$U-B$ (mag)	$\sigma(U-B)$ (mag)	n_{UB}	$B-V$ (mag)	$\sigma(B-V)$ (mag)	n_{BV}	$V-I$ (mag)	$\sigma(V-I)$ (mag)	n_{VI}
	–	–	–	–	–	–	–	–	–	–	–	–	–	–
10	177.685	350.761	12.449	0.009	3	0.044	0.015	3	0.556	0.020	3	0.552	0.027	3
11	1886.703	2012.226	12.558	0.013	3	0.100	0.025	3	0.495	0.026	3	0.528	0.034	3
12	1131.933	6.053	12.597	0.025	3	−0.055	0.009	3	0.460	0.016	3	0.491	0.050	3
	–	–	–	–	–	–	–	–	–	–	–	–	–	–

NOTE: (x,y) coordinates correspond to the reference system of Fig. 1. Magnitude and colour errors are the standard deviations of the mean or the observed photometric errors for stars with only one measurement.

Table 5
CCD *UBVI* data of stars in the field of NGC 2368.

ID	x (pix)	y (pix)	V (mag)	$\sigma(V)$ (mag)	n_V	$U-B$ (mag)	$\sigma(U-B)$ (mag)	n_{UB}	$B-V$ (mag)	$\sigma(B-V)$ (mag)	n_{BV}	$V-I$ (mag)	$\sigma(V-I)$ (mag)	n_{VI}
	–	–	–	–	–	–	–	–	–	–	–	–	–	–
951	1504.014	659.479	19.047	0.002	2	0.530	0.006	2	1.020	0.008	2	1.278	0.002	2
952	1964.566	877.993	18.621	0.008	2	0.842	0.016	2	1.157	0.007	2	1.138	0.008	2
953	1078.364	2041.205	18.982	0.008	2	0.440	0.012	2	1.093	0.003	2	1.173	0.008	2
	–	–	–	–	–	–	–	–	–	–	–	–	–	–

NOTE: (x,y) coordinates correspond to the reference system of Fig. 1. Magnitude and colour errors are the standard deviations of the mean or the observed photometric errors for stars with only one measurement.

Table 6
CCD *BV* data of stars in the field of Haffner 25.

ID	x (pix)	y (pix)	V (pix)	$\sigma(V)$ (mag)	n_V	$B-V$ (mag)	$\sigma(B-V)$ (mag)	n_{BV}
	–	–	–	–	–	–	–	
12	1108.291	9.780	19.015	0.001	2	0.991	0.019	2
13	1871.356	10.017	14.465	0.001	2	1.372	0.071	1
14	267.641	11.631	19.744	0.001	2	1.764	0.089	1
	–	–	–	–	–	–	–	–

NOTE: (x,y) coordinates correspond to the reference system of Fig. 1. Magnitude and colour errors are the standard deviations of the mean or the observed photometric errors for stars with only one measurement.

Table 7
CCD *UBVI* data of stars in the field of Hogg 3 and Hogg 4.

ID	x (pix)	y (pix)	V (pix)	$\sigma(V)$ (mag)	n_V	$U-B$ (mag)	$\sigma(U-B)$ (mag)	n_{UB}	$B-V$ (mag)	$\sigma(B-V)$ (mag)	n_{BV}	$V-I$ (mag)	$\sigma(V-I)$ (mag)	n_{VI}
	–	–	–	–	–	–	–	–	–	–	–	–	–	–
9	921.469	4.865	17.649	0.036	6	0.612	0.007	2	1.228	0.022	3	1.409	0.059	6
10	11.712	4.571	18.329	0.036	2	0.620	0.095	1	1.467	0.041	1	1.607	0.056	2
11	935.596	6.228	17.996	0.031	4	0.138	0.041	2	1.256	0.045	3	1.416	0.038	4
	–	–	–	–	–	–	–	–	–	–	–	–	–	–

NOTE: (x,y) coordinates correspond to the reference system of Fig. 1. Magnitude and colour errors are the standard deviations of the mean or the observed photometric errors for stars with only one measurement.

V = 18, 19 and 20 mag, respectively. The stars with two measures of $U-B$, $B-V$ and $V-I$ colours cover V ranges from 16.0 to 19.5 mag, from 17.0 to 20.0 mag and from 18.0 to 21 mag, respectively. Finally, the stars with only one measure of $U-B$, $B-V$ and

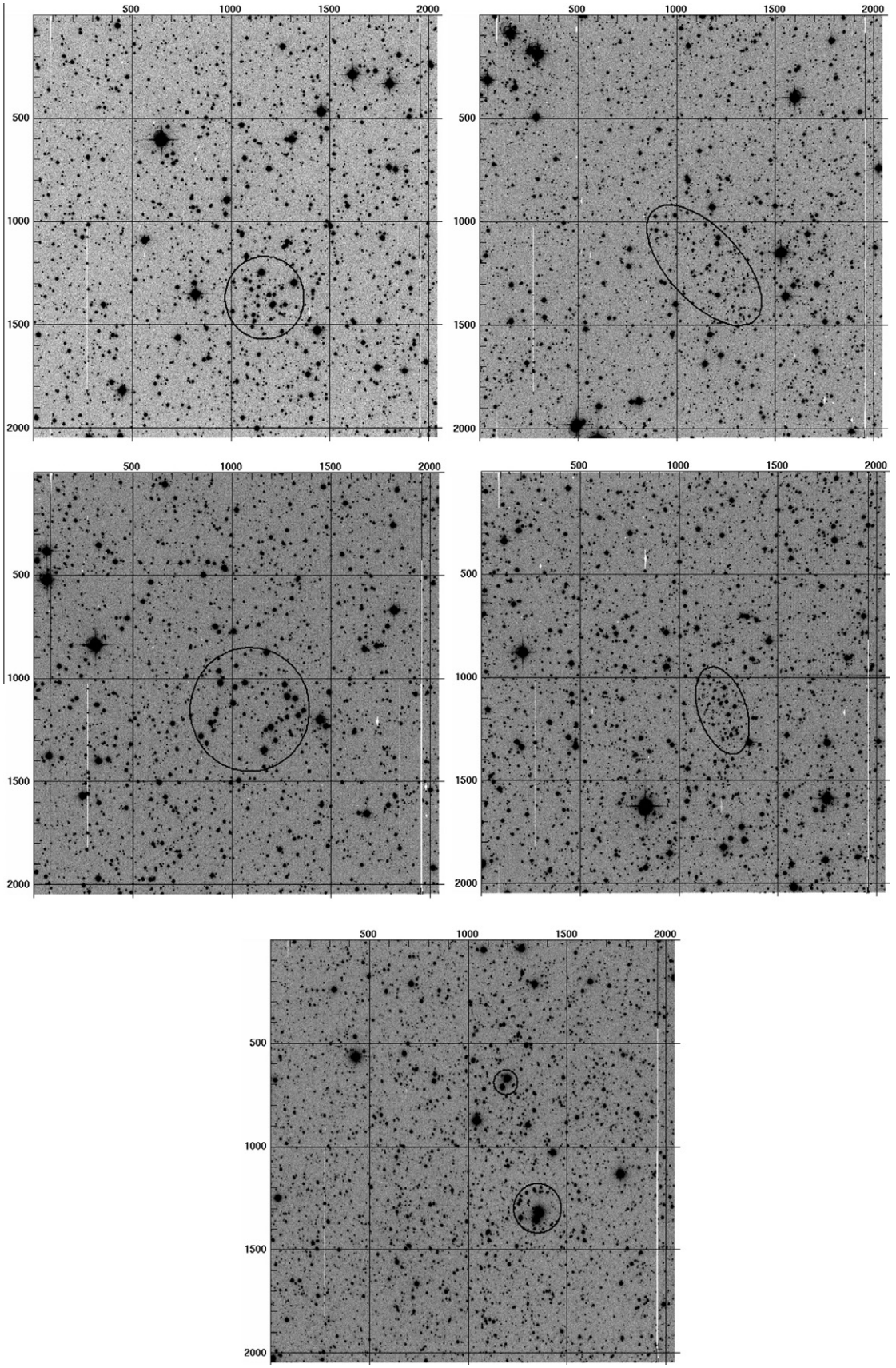

Fig. 1. Deepest CCD images obtained: 200 s *V* for Haffner 3 (*top left*); 200 s *V* for Haffner 5 (*top right*); 200 s *V* for NGC 2368 (*middle left*); 200 s *V* for Haffner 25 (*middle right*); and 200 s *V* for Hogg 3 and Hogg 4 (*bottom*). North is up and East is to the left. Coordinates are given in pixels.

Table 8
Magnitude and colour photometric errors as a function of V.

Δ V (mag)	$\sigma(V)$ (mag)	$\sigma(U\cdot B)$ (mag)	$\sigma(B\cdot V)$ (mag)	$\sigma(V\cdot I)$(mag)
11.12	< 0.01	0.01	< 0.01	< 0.01
12.13	< 0.01	0.02	0.01	0.01
13.14	< 0.01	0.02	0.01	0.01
14.15	0.01	0.03	0.01	0.02
15.16	0.01	0.04	0.01	0.02
16.17	0.02	0.04	0.02	0.02
17.18	0.02	0.05	0.02	0.03
18.19	0.03	0.06	0.03	0.03
19.20	0.03	0.07	0.05	0.05
20.21	0.05	0.10	0.10	0.10
21.22	0.10	–	–	0.15

$V-I$ are fainter than V = 18.0, 19.0 and 20.0 mag, respectively, and reach the photometric magnitude limits. This statistics makes it clear that the stars lying within the ∼6 brightest out of the ∼9 mag range along which our photometry extends were measured two and three times. Therefore, these stars are the most appropriate ones to derive astrophysical information. The behaviour of the photometric errors for the V magnitude and $U-B$, $B-V$ and $V-I$ colours as a function of V is shown in Table 8. We used all the observed stars since those measured only once have practically no statistical weight. According to Table 8 and to the above mentioned statistics, we believe it is possible to rely on the accuracy of the morphology of the main features in both the colour–magnitude diagrams (CMDs) and the colour–colour diagrams (CCDs). The resulting CMDs and CCDs are drawn in Figs. 2–6 which show, in general, broad star sequences. Since we only obtained B and V images in the Haffner 25 field, we just show the (V,$B-V$) CMD for this object.

3. Data analysis

On inspecting Fig. 1, a possible OC might be identified by a concentration of a handful of bright stars that stand out from a slightly fainter surrounding field, by a visible increase in the stellar population in a sky region or even by both features combined. Occasionally, however, apparent concentrations of bright stars located approximately along the same direction or even variations in the number of stars – caused by the presence of interstellar clouds – can lead to the identification of unreal OCs.

We analysed the possible existence of genuine OCs in the studied fields following two different approaches. On the one hand, we examined the distribution of stars in the CMDs and CCDs and, on the other hand, we compared the number of stars counted within and outside the fields of the cluster candidates. A complementary analysis of both approaches will allow us to confirm or deny, on sounder bases, the physical reality of these objects.

3.1. CMDs and CCDs

Without a careful analysis of the observed sequences in the CMDs, one might conclude that such sequences are in fact clusters' main sequences (MSs). However, all the CMDs present different MSs more or less superimposed. This means that the different MSs could be affected by nearly similar reddenings, which makes it difficult to disentangle their own features and renders the analysis of the CMDs challenging. Fortunately, the availability of CCDs involving the $U-B$ colour greatly helps us to successfully perform this task.

To estimate a magnitude from which the characteristics of the different observed MSs are undistinguishable in terms of spatial

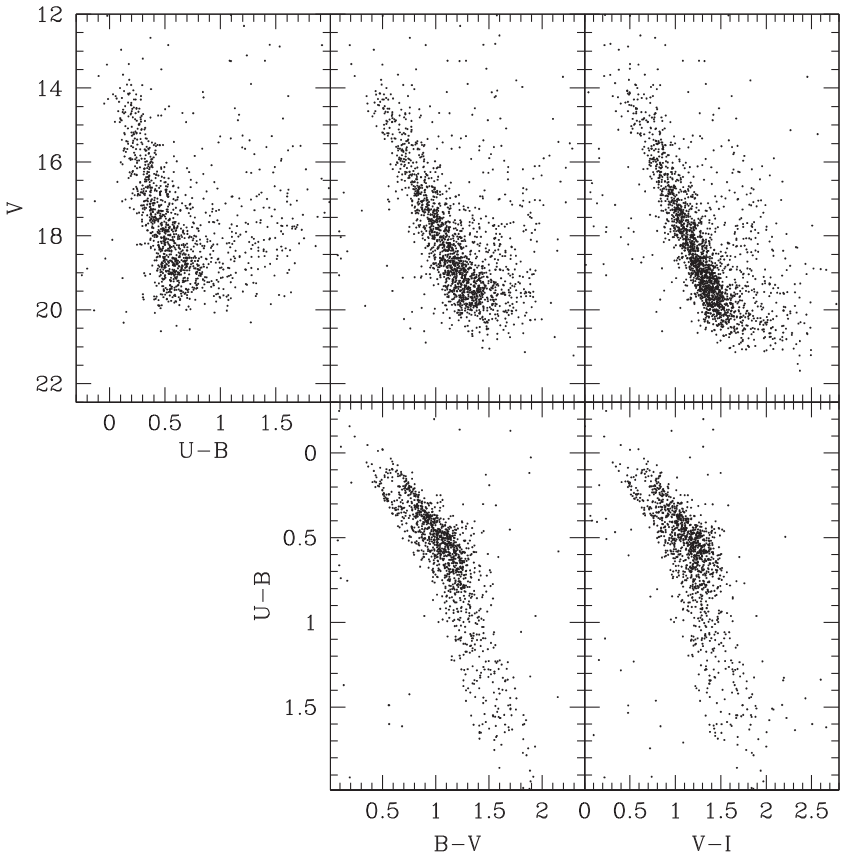

Fig. 2. The (V, $U\cdot B$), (V,$B\cdot V$), and (V,$V\cdot I$) diagrams (*top*), and ($U\cdot B$,$B\cdot V$) and ($B\cdot V$,$V\cdot I$) diagrams (*bottom*) for the stars measured in the field of Haffner 3.

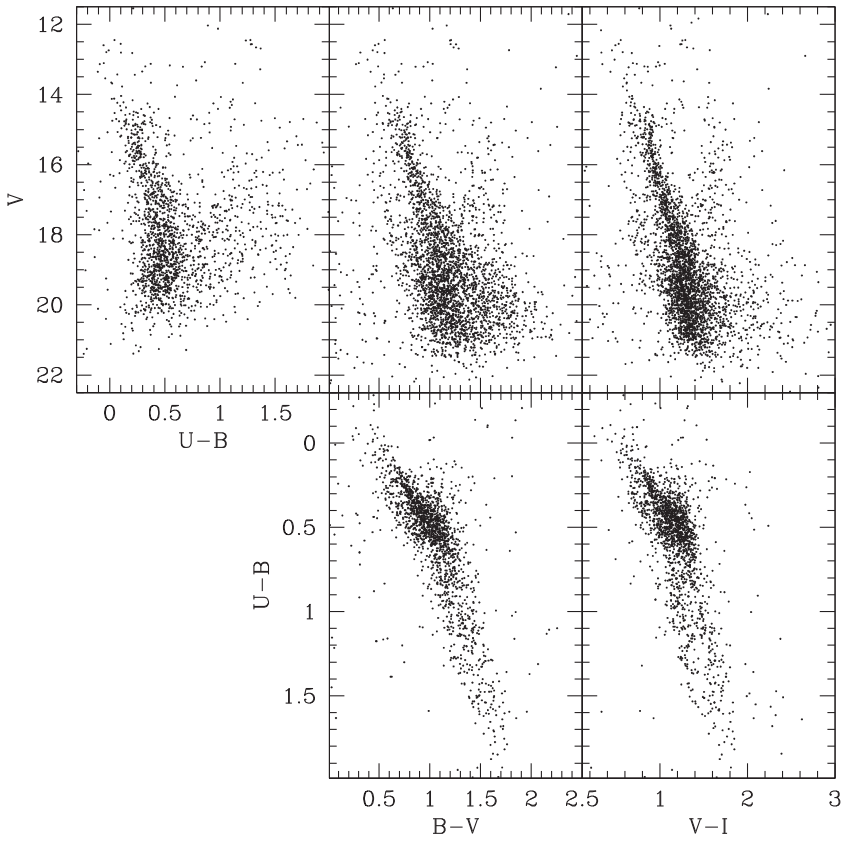

Fig. 3. The $(V,U\cdot B)$, $(V,B\cdot V)$, and $(V,V\cdot I)$ diagrams (*top*), and $(U\cdot B,B\cdot V)$ and $(B\cdot V,V.I)$ diagrams (*bottom*) for the stars measured in the field of Haffner 5.

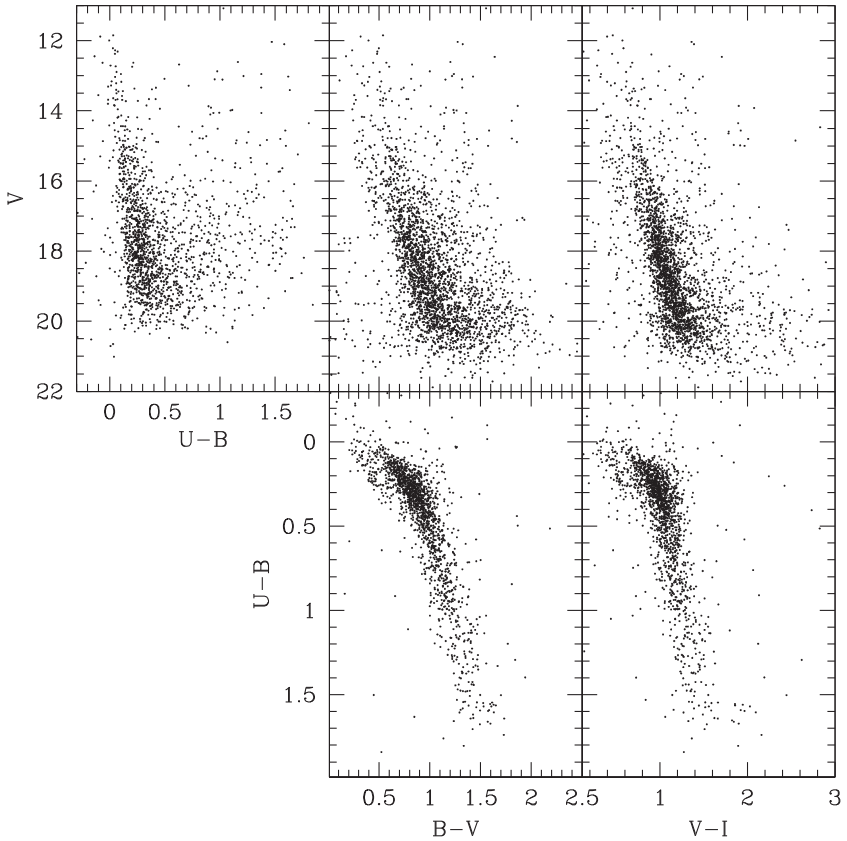

Fig. 4. The $(V,U\cdot B)$, $(V,B\cdot V)$, and $(V,V\cdot I)$ diagrams (*top*), and $(U\cdot B,B\cdot V)$ and $(B\cdot V,V\cdot I)$ diagrams (*bottom*) for the stars measured in the field of NGC 2368.

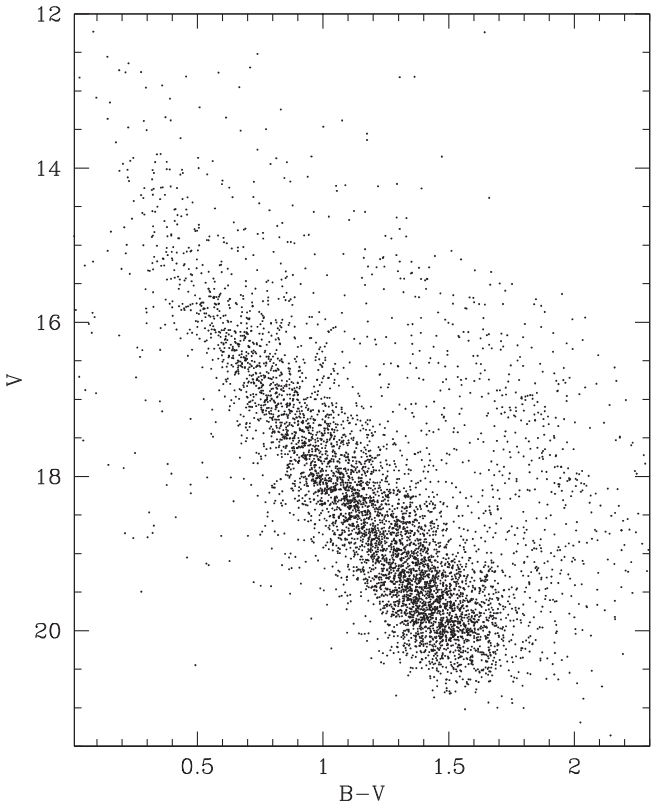

Fig. 5. The $(V,B\cdot V)$ diagrams for the stars measured in the field of Haffner 25.

density, magnitude and colour distributions, we applied a statistical method. Such method permitted us to filter the field stars from the CMDs and CCDs. Then, we divided the observed region into 64 non-overlapped boxes of 250 pixels a side and built, for each of them, the corresponding CMDs. This procedure consists of alternatively adopting as reference any of the box extracted CMDs to statistically filter the remaining ones. We repeated this filtering task using each of the box extracted CMDs as a reference CMD. The filtering was performed in such a way that we counted how many stars lie in different magnitude–colour bins sized $(\Delta V,\Delta(U-B)=\Delta(B-V)=\Delta(V-I))=(0.5,0.2)$ mag. Next, we subtracted from each CMD the number of stars counted for each range of the reference CMDs. We did this by removing those stars closer in magnitude and colour to the ones of the CMD used as reference. In order to compare the resulting residuals, we performed the filtering procedure by using bins of $(1.0,0.2)$ mag and $(0.5,0.1)$ mag as well as boxes of 500×500 pixels.

By comparing the various filtered CMDs corresponding to a given box with the observed one, the residuals from box-to-box variations and the fiducial CMD features of that box could be found. This is due to the fact that a star that has magnitude and colours within the typical values obtained in the reference field CMDs is, in most cases, eliminated. Therefore, the fewer times a star is removed in a given box, the larger its probability of representing a fiducial feature in that box. So we adopted every star that was removed fewer than 20 per cent of the times as a probable fiducial feature star. In this way, it became clear to us that our photometry does not permit to distinguish different MSs for V magnitudes fainter than $\sim$16.

Bearing in mind this result, the criteria adopted for evaluating the membership status of the measured stars are those defined

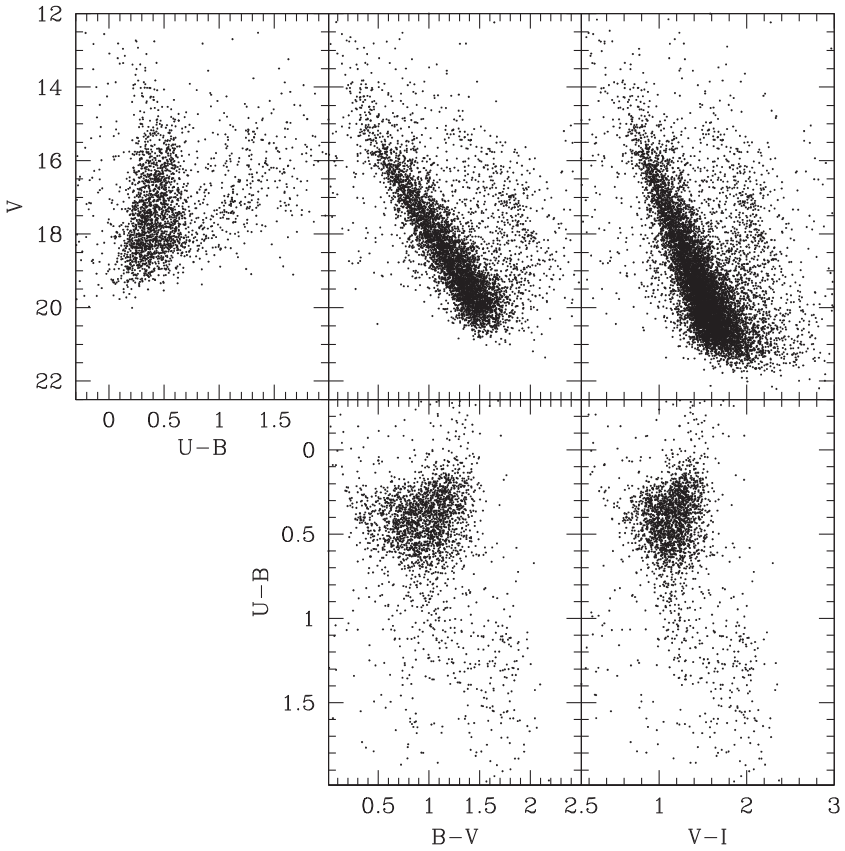

Fig. 6. The $(V,U\cdot B)$, $(V,B\cdot V)$, and $(V,V\cdot I)$ diagrams (*top*), and $(U\cdot B,B\cdot V)$ and $(B\cdot V,V\cdot I)$ diagrams (*bottom*) for the stars measured in the field of Hogg 3 and Hogg 4.

Table 9
Estimated parameters for the observed fields.

	Haffner 3	Haffner 5	NGC 2368	Haffner 25	Hogg 3	Hogg 4
$E(B-V)_{SFD}$ (mean)	0.87 ± 0.02	0.68 ± 0.04	0.45 ± 0.01	0.53 ± 0.03	1.38 ± 0.05	1.38 ± 0.05
$E(B-V)_{SFD}$ (min.)	0.85	0.62	0.43	0.49	1.32	1.32
$E(B-V)_{SFD}$ (max.)	0.91	0.74	0.47	0.59	1.48	1.48
Stars/box (mean)	20 ± 13	31 ± 15	25 ± 10	31 ± 16	98 ± 37	98 ± 37
Stars/box (object)	36	34	35	50	110	110
R^2/box (mean)	11 ± 13	15 ± 9	12 ± 10	17 ± 13	45 ± 23	45 ± 23
R^2/box (object)	20	27	20	24	64	54

by Clariá and Lapasset (1986). Firstly, it is required that the location of a star in the two CCDs is close to the MS of the cluster, the maximum accepted deviation being 0.10 mag. The second requirement is that the location of the same star in the three CMDs corresponds to the same evolutionary stage.

To identify what stars fulfill the criteria stated above, we superimposed the zero-age main sequence (ZAMS) of Lejeune and Schaerer (2001) to the observed $(U-B,B-V)$ diagram by adopting a colour excess $E(B-V)=E_o$; then, we looked for every star closer than 0.10 mag from the ZAMS. The value E_o corresponds to the bluest envelope of the observed sequence. The location of the ZAMS in this $(U-B,B-V)$ diagram also requires the knowledge of the slope of the reddening line. It is well known, however, that there are variations in the reddening law throughout the Galaxy (Turner, 1994), although a mean reddening slope of $E(U-B)/E(B-V)=0.72$ is usually found for most Galactic longitudes. If we adopt $E(V-I)/E(B-V)=1.25$ (Dean et al., 1978), this value implies the following ratio: $E(U-B)/E(V-I)=0.72/1.25=0.58$. Thus, by sliding the ZAMS according to this reddening line in the $(U-B,V-I)$ diagram, we discarded as cluster members all stars that fall beyond 0.10 mag from the ZAMS. Then, using all the stars that complied with this first requirement, we kept as probable members those stars whose locations correspond to the same evolutionary stage in the three CMDs. For that purpose, we superimposed the ZAMS to the three CMDs by adopting the above $E(B-V)$ value using the apparent distance modulus $m-M$ which best fits the ZAMS to the unevolved star sequence. Finally, by carefully inspecting the three CMDs and the two CCDs, we could distinguish the possible cluster stars. We repeated this procedure for different $E(B-V)$ values that we increased in steps of 0.05 mag each time. Although some star sequences seem to delineate a cluster MS in both CCDs, they are composed of field stars more or less aligned along the sight of view, since none of them have their counterpart MS in the three CMDs. These results allow us to conclude that the six studied objects would not be genuine OCs.

The method described presupposes that the colour excesses are uniform across the observed fields. Nevertheless, sometimes the colour excesses in certain regions of the sky are not uniform at all and the presence of real OCs in these cases could be hidden by the existence of differential reddening. We used the reddening maps of Schlegel et al. (1998, hereafter SFD) to corroborate our assumption. SFD obtained full-sky maps from 100 μm dust emission. They found that in high Galactic latitude regions, the dust map correlates well with maps of H I emission. However, deviations are coherent in the sky and are especially conspicuous in regions of H I emission saturation towards denser clouds and in regions of formation of H_2 in molecular clouds (Piatti et al., 2003, 2008). Even if the SFD's reddenings were not totally correct, it may still be useful to consider their values for the observed fields. We used the NASA/IPAC Infrared Science Archive to extract the $E(B-V)_{SFD}$ reddenings from a 2° wide image (the minimum size available) centred on the objects. The resulting $E(B-V)_{SFD}$ colour excesses are shown in Table 9. Since these values turned out to be considerably larger than any value expected from the observed $(U-B,B-V)$ diagrams, we assumed that the $E(B-V)_{SFD}$ values must be saturated. It is worth considering that the range of $E(B-V)_{SFD}$ values for each field is <0.12 mag (except for Hogg 3 and Hogg 4, which is 0.16), slightly larger than 0.11, the lowest limit estimated by Burki (1975) for clusters with differential reddening. So we conclude that the interstellar reddening across the observed fields can be considered uniform within the quoted uncertainties.

3.2. Star counts

At first, we estimated the mean stellar density representative of each observed field by fitting Gaussian distributions to the star counts in 100 non-overlapped boxes of 200 pixels a side. The fits of the Gaussians were performed using the NGAUSSFIT routine in the STSDAS/IRAF[2] package. We adopted a single Gaussian and fixed the linear terms to zero and the constant to the corresponding background level. The resulting average numbers of stars per box with the corresponding standard deviations are shown in the fourth line of Table 9. In the fifth line, we included the number of stars in a box of 200×200 pixels centred on the suspected clusters. As these last values lie within 1.2σ of the mean values, they do not favour the possibility that the studied objects are real physical aggregates.

A real OC is sometimes composed by stars more or less sparsed in a relatively large area of the sky or it may contain only a handful of comparatively bright stars. In such cases, the stellar density alone could not be a meaningful indicator of the presence of an OC. For this reason, we decided to statistically clean the CMDs from stars that can potentially belong to the foreground/background fields. We built star field CMDs using the stars located in the easternmost strip of the observed fields, i.e., $x<500$ pixels and $0<y$ (pixels) <2050 (see, Fig. 1). We treated separately the CMDs for $U-B$, $B-V$ and $V-I$. Using these field CMDs, we counted how many stars lay in different magnitude–colour bins with sizes $[\Delta V,\Delta(U-B)=\Delta(B-V)=\Delta(V-I)]=(0.5,0.1)$ mag. We then subtracted from each CMD the number of stars counted for each range in the field $[V,(U-B,B-V$ or $V-I)]$ CMDs, by removing those stars closer in magnitude and colour to the ones in the star fields.

Although the cleaning process was applied to an extended region surrounding the catalogued objects ($x>500$ pixels and $0<y$ (pixels) <2050), Figs. 7–12 show with filled circles the circular/elliptical extracted CMDs and CCDs that were obtained after cleaning them for field star contamination. In these figures, we show overplotted the CMDs and CCDs directly obtained with all the measured stars in those circular/elliptical regions (dots). When comparing observed and cleaned CMDs and CCDs, the differences in stellar composition did not become evident. The circular/elliptical regions were visually defined on the images of Fig. 1 taking into account the object equatorial coordinates, their morphological characteristics (e.g., Trumpler class, etc) and our somewhat subjective criterion of encompassing what we think should be their main

[2] IRAF is distributed by the National Optical Astronomy Observatories, which is operated by the Association of Universities for Research in Astronomy, Inc., under contract with the National Science Foundation

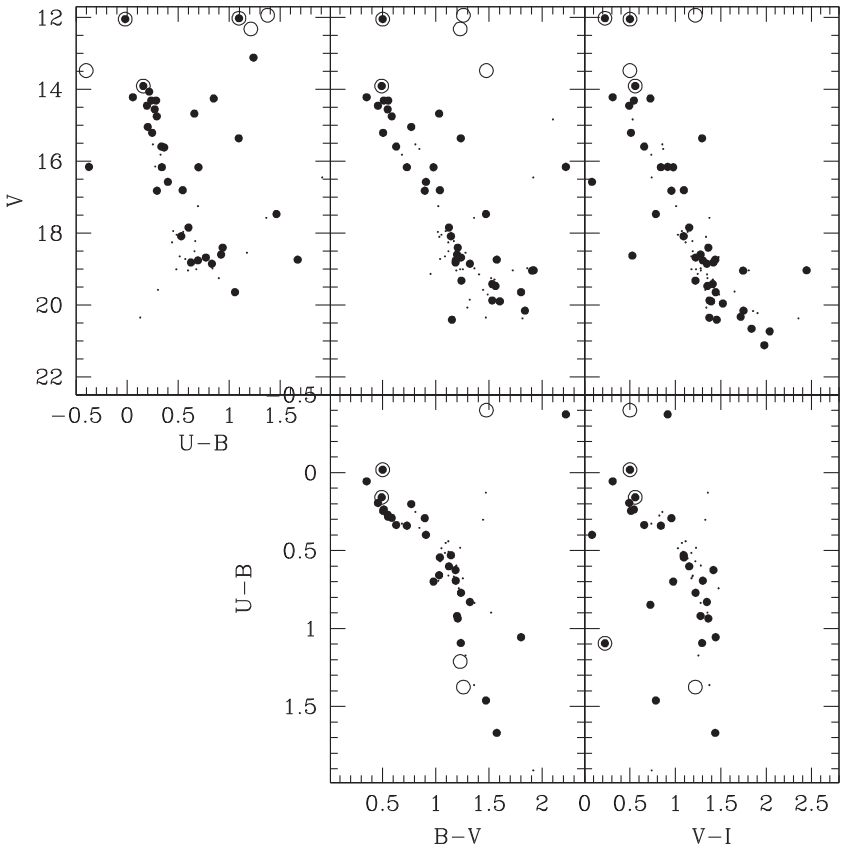

Fig. 7. The extracted (V,$U-B$), (V,$B-V$), and (V,$V-I$) diagrams (*top*), and extracted ($U-B$,$B-V$) and ($B-V$,$V-I$) diagrams (*bottom*) for the Haffner 3 circular region of Fig. 1 (dots), compared with those statistically cleaned from field star contamination (filled circles). Open circles represent stars of the northern group according to Babu (1983).

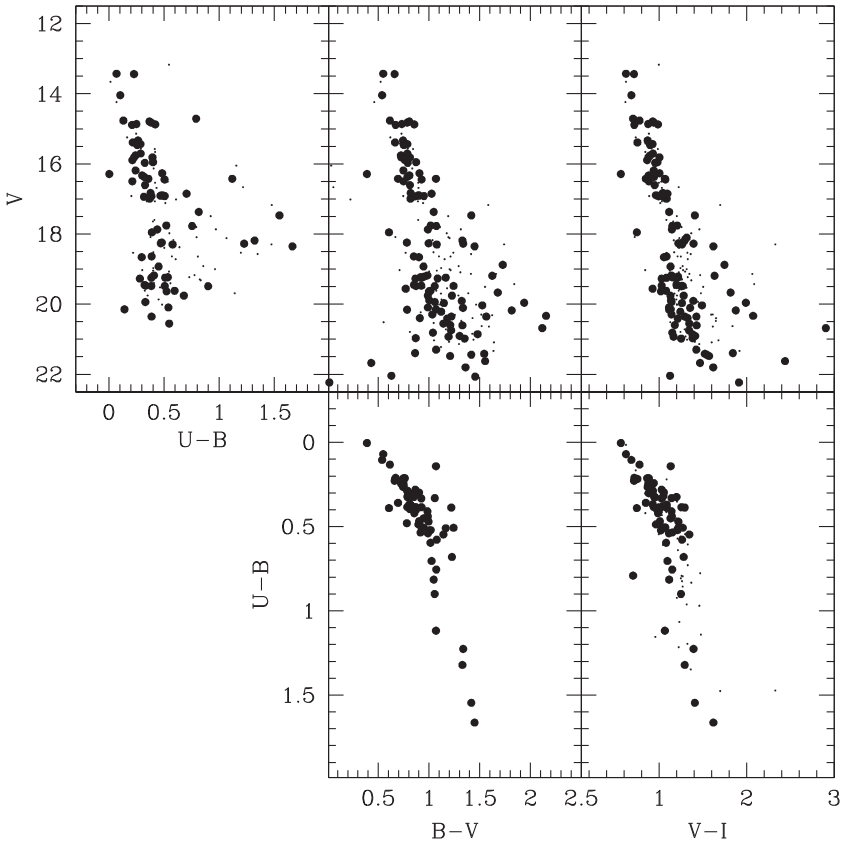

Fig. 8. The extracted (V,$U-B$), (V,$B-V$), and (V,$V-I$) diagrams (*top*), and extracted ($U-B$,$B-V$) and ($B-V$,$V-I$) diagrams (*bottom*) for the Haffner 5 elliptical region of Fig. 1 (dots), compared with those statistically cleaned from field star contamination (filled circles).

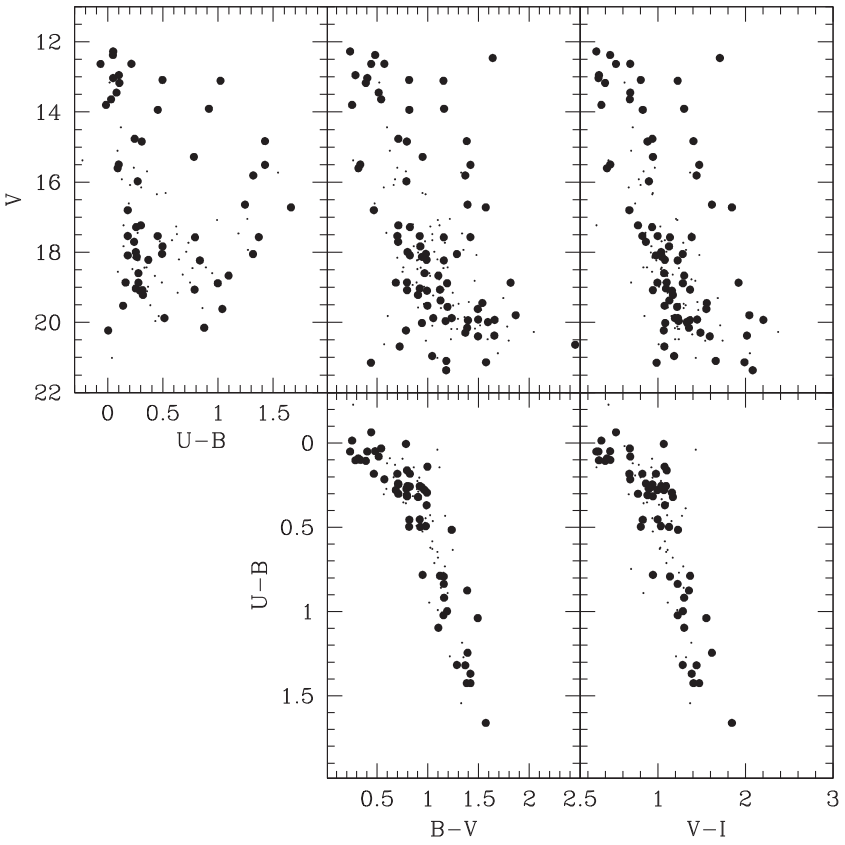

Fig. 9. The extracted $(V,U\cdot B)$, $(V,B\cdot V)$, and $(V,V\cdot I)$ diagrams (*top*), and extracted $(U\cdot B,B\cdot V)$ and $(B\cdot V,V\cdot I)$ diagrams (*bottom*) for the NGC 2368 circular region of Fig. 1 (dots), compared with those statistically cleaned from field star contamination (filled circles).

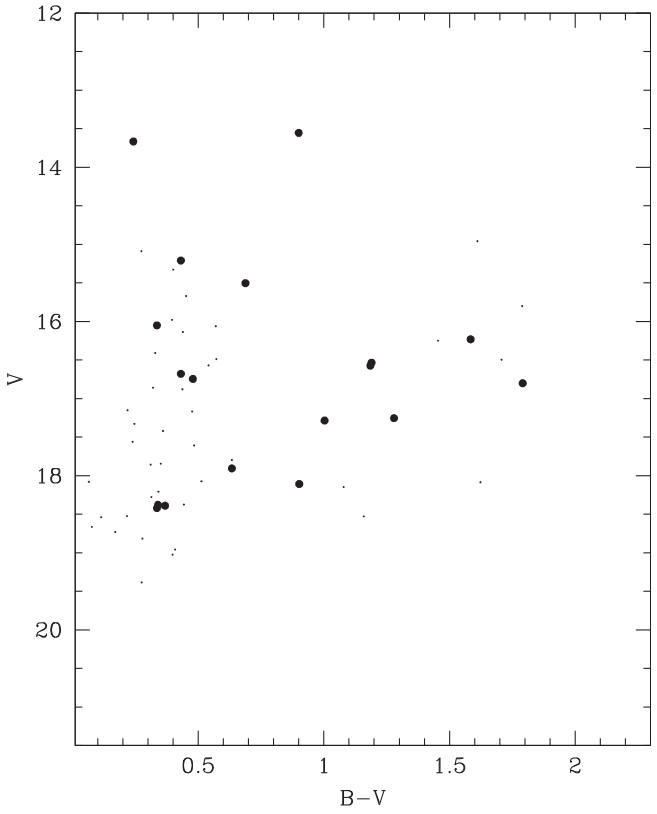

Fig. 10. The extracted $(V,B\cdot V)$ diagram for the Haffner 25 elliptical region of Fig. 1 (dots), compared with that statistically cleaned from field star contamination (filled circles).

bodies. Keeping in mind that field stars may give rise to well defined sequences in the CMDs, the presence of such sequences must not be considered in itself a proof of the existence of an OC (Burki and Maeder, 1973). This becomes an additional difficulty when the cluster CMDs are cleaned. Sequences of observed field stars may be discriminated from those of real OCs for the following three reasons: (i) the former show a limiting envelope of different curvature, (ii) the field stars have incompatible positions in the various CMDs, (iii) the field apparent luminosity function reaches its maximum at the observed limiting magnitude. Figs. 7–12 allow us to come to the conclusion that the six observed objects are not genuine OCs.

Profiting from the above described cleaning process, we applied the method of Pavani and Bica (2007) to measure how different the stellar densities encompassed by the adopted circles/ellipses are from the field star density. Pavani and Bica (2007) defined the R^2 statistics that reflects the distribution of field fluctuations and stellar density contrast in the CMD between those of the clusters and those in the star field. We thus built nearly a hundred CMDs for different boxes of 200×200 pixels distributed throughout the field, in addition to the CMDs for the catalogued objects (Figs. 7–12). We computed R^2 for each box, then built the histograms of the R^2 distributions for each observed field and performed Gaussian fits for each of them. The resulting R^2 averaged values and their corresponding dispersions are listed in line six of Table 9. We found that the R^2 values for the catalogued objects (line seven of Table 9) do not exceed in more than 1σ the mean value derived for their respective fields, except in the case of Haffner 5 whose value is 1.3σ. These results imply that none of the six catalogued objects constitute genuine physical systems or OC remnants but should rather be considered random fluctuations of the field star density.

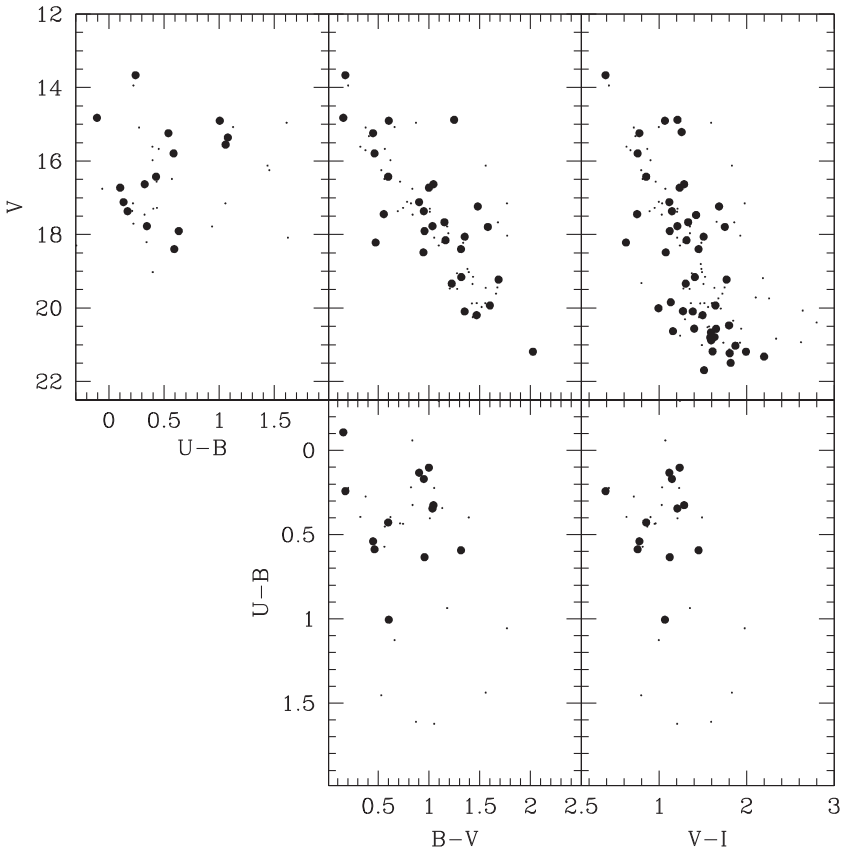

Fig. 11. The extracted ($V, U-B$), ($V, B-V$), and ($V, V-I$) diagrams (*top*), and extracted ($U-B, B-V$) and ($B-V, V-I$) diagrams (*bottom*) for the Hogg 3 circular region of Fig. 1 (dots), compared with those statistically cleaned from field star contamination (filled circles).

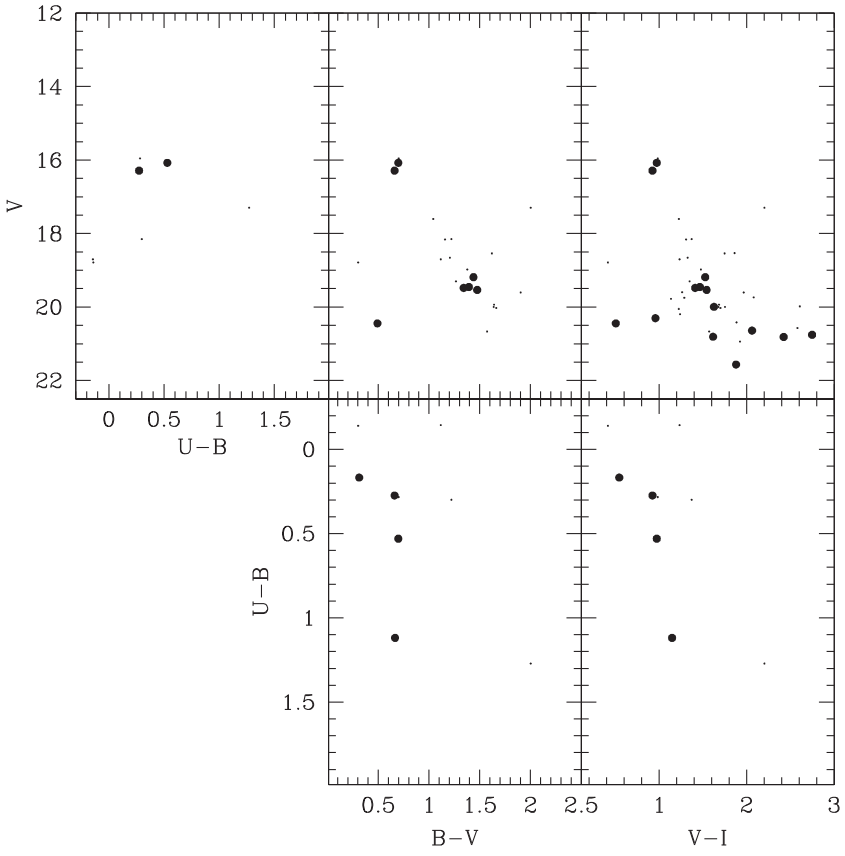

Fig. 12. The extracted ($V, U-B$), ($V, B-V$), and ($V, V-I$) diagrams (*top*), and extracted ($U-B, B-V$) and ($B-V, V-I$) diagrams (*bottom*) for the Hogg 4 circular region of Fig. 1 (dots), compared with those statistically cleaned from field star contamination (filled circles).

3.3. Previous results

Considering Haffner 3, NGC 2368 and Hogg 3 real OCs, Ahumada et al. (2001) determined their fundamental parameters. They estimated the basic parameters of NGC 2368 and Hogg 3 from the comparison of the observed integrated cluster spectra with template spectra of OCs with well known fundamental parameters, as well as from the measurements of the Balmer line equivalent widths. They derived for NGC 2368 and Hogg 3 ages of about 50–100 Myr and $E(B-V) = 0.12$ and 0.15 from template matching, respectively, while the ages obtained from the Balmer lines turned out to be only slightly younger. Ahumada et al. (2001) found the spectral features of Hogg 3 quite similar to those of the also observed, less reddened cluster Hogg 12. We believe that very probably the integrated spectra reflect the combined light produced by comparatively bright foreground stars so that the parameters derived from such spectra should be regarded as representative of those foreground stars. We think that the integrated spectroscopic technique becomes a powerful tool only in cases in which the observed object has a very small angular diameter.

Babu (1983) obtained low-dispersion spectra for 22 stars in the field of Haffner 3 from which he determined spectral types and membership status. He mentioned the interesting feature that there are two distinct concentrations or physical groups separated by a small region of low star density (see his Fig. 16). Fig. 7 shows Babu's members of the northern group, represented by open circles in our CMDs and CCDs. The 7 members of the southern group fall outside the observed field of view (FOV). We only have photometry for six out of the nine Babu's northern members: stars 8, 11, 12, 14, 15 and 21. Star 6 falls outside the FOV, star 10 appears to be saturated and star 25 was not measured by us. As can be seen in Fig. 7, those six northern group stars do not exhibit the typical features of an OC.

4. Summary and conclusions

New CCD $UBVI_{KC}$ photometry in the field of the stellar aggregates Haffner 3, Haffner 5, NGC 2368, Haffner 25, Hogg 3 and Hogg 4 is reported here. All these objects are included in different OC catalogues (Alter et al., 1970, 1987; Dias et al., 2002). The analysis of the current photometric data leads to the following main conclusions:

(i) None of the observed CMDs and CCDs reveal the presence of the MS of an OC. The different observed CMDs reveal the apparent superposition of MS or giant field stars affected by various amounts of interstellar absorption. Those field stars are located at different distances from the Sun.

(ii) The observed CMDs of the six OC candidates cleaned from field star contamination were built by statistically subtracting the number of stars counted in their respective field CMDs. The stars closer in magnitude and colour to the ones in the respective star fields were thus removed. The resulting cleaned CMDs show MSs whose lower envelopes are not those corresponding to real OCs.

(iii) We discussed the possible physical nature of the six studied objects by checking whether or not they present a significant number density contrast with respect to the Galactic disk. Star counts performed within and outside the cluster candidate fields not only support the results inferred from the CMDs and CCDs but also suggest that the studied objects are not OC remnants.

(iv) Several other stellar aggregates included in OC catalogues have previously been discarded as genuine physical systems (see, e.g., Carraro and Patat, 1995; Carraro, 2000; Piatti and Clariá, 2001b). The present study reveals the need for further research of poorly studied or unstudied catalogued OCs in order to clarify their nature.

Acknowledgements

We are gratefully indebted to the CTIO staff for their hospitality and support during the observing run. This work was partially supported by the Argentinian institutions CONICET, SECYT (Universidad Nacional de Córdoba) and Agencia Nacional de Promoción Científica y Tecnológica (ANPCyT). This work is based on observations made at Cerro Tololo Inter-American Observatory, which is operated by AURA, Inc., under cooperative agreement with the National Science Foundation. This research has made use of the SIMBAD database, operated at CDS, Strasbourg, France; also the WEBDA database, operated at the Institute for Astronomy of the University of Vienna, and the NASA's Astrophysics Data.

Appendix A. Supplementary data

Supplementary data associated with this article can be found, in the online version, at doi:10.1016/j.newast.2010.08.009.

References

Ahumada, A.V., Clariá, J.J., Bica, E., Dutra, C.M., Torres, M.C., 2001. A& A 377, 845.
Alter, G., Ruprecht, J., Vanisek, J., 1970. Catalogue of Star Clusters and Associations. Akademiai Kiado, Budapest.
Archinal, B.A., Hynes, S.J., 2003. Star Clusters. Willman-Bell, Richmond VA.
Babu, G.S.D., 1983. J. Astrophys. Astr. 4, 235.
Bassino, L.P., Waldhausen, S., Martínez, R.E., 2000. A& A 355, 138.
Bica, E., Santiago, B.X., Dutra, C.M., et al., 2001. A& A 827, 833.
Burki, G., Maeder, A., 1973. A& A 25, 71.
Carraro, G., 2000. A& A 357, 145.
Carraro, G., Patat, F., 1995. MNRAS 276, 563.
Clariá, J.J., Lapasset, E., 1986. AJ 91, 326.
Collinder, P., 1931. MeLu2.
de la Fuente Marcos, R., 1998. A& A 333, L27.
Dean, F.J., Warren, P.R., Cousins, A.W.J., 1978. MNRAS 183, 569.
Dias, W.S., Alessi, B.S., Moitinho, A., Lepine, J.R.D., 2002. A& AS 141, 371.
Landolt, A., 1992. AJ 104, 340.
Lauberts, A., 1982. In ESO/Uppsala survey of the ESO(B) atlas, Garching: European Southern Observatory (ESO).
Lejeune, T., Schaerer, D., 2001. A& A 366, 538.
Lyngå, G., 1987. Catalogue of Open Cluster Data. Centre de Données Stellaires, Strasbourg.
Pavani, B., Bica, E., 2007. A& A 468, 139.
Piatti, A.E., Bica, E., Clariá, J.J., 2000. A& A 362, 959.
Piatti, A.E., Clariá, J.J., 2001a. A& A 370, 931.
Piatti, A.E., Clariá, J.J., 2001b. A& A 379, 453.
Piatti, A.E., Clariá, J.J., Ahumada, A.V., 2009. MNRAS 397, 1073.
Piatti, A.E., Clariá, J.J., Bica, E., 2000. A& A 360, 529.
Piatti, A.E., Clariá, J.J., Bica, E., Geisler, D., Minniti, D., 1998. AJ 116, 801.
Piatti, A.E., Geisler, D., Bica, E., Clariá, J.J., 2003. MNRAS 343, 851.
Piatti, A.E., Geisler, D., Sarajedini, A., Gallart, C., Wischnjewsky, M., 2008. MNRAS 389, 429.
Schlegel, D.J., Finkbeiner, D.P., Davis, M., 1998. ApJ 500, 525. SFD.
Trumpler, R.J., 1930. LicOB 14, 154.
Turner, D.G., 1994. RMAA 29, 163.